Final Report

AN INVESTIGATION OF COMBUSTION INSTABILITY IN HYBRID ROCKETS

Prepared for:

NATIONAL AERONAUTICS AND SPACE ADMINISTRATION
LANGLEY RESEARCH CENTER
HAMPTON, VIRGINIA

CONTRACT NAS1-9319

(NASA-CR-155074) AN INVESTIGATION OF COMBUSTION INSTABILITY IN HYBRID ROCKETS Final Report (Stanford Research Inst.) 44 p

N77-85560

00/20 Unclas 15075

STANFORD RESEARCH INSTITUTE
Menlo Park, California 94025 · U.S.A.

STANFORD RESEARCH INSTITUTE
Menlo Park, California 94025 · U.S.A.

Final Report *March 6, 1970*

AN INVESTIGATION OF COMBUSTION INSTABILITY IN HYBRID ROCKETS

By: C. E. WOOLDRIDGE and R. J. KIER

Prepared for:

NATIONAL AERONAUTICS AND SPACE ADMINISTRATION
LANGLEY RESEARCH CENTER
HAMPTON, VIRGINIA 23365

Attention: MR. WILLIAM P. PECK
MAIL STOP 498

CONTRACT NAS1-9319

SRI Project PHU-8060

Approved:

E. M. KINDERMAN, *Director*
Applied Physics Laboratory

C. J. COOK, *Executive Director*
Physical Sciences Division

i

ABSTRACT

A simple analysis has been developed to describe the transition of hybrid rocket combustion from the diffusion-limited region at high pressure to the kinetic-limited domain at low pressure. Good qualitative agreement has been obtained with measured regression rate behavior in those operating regimes where surface effects such as excessive melting or charring do not occur.

PREFACE

The studies described in this report were performed principally by C. E. Wooldridge (theory) and R. J. Kier (experiments). The overall program has been under the direction of G. A. Marxman.

Administration and technical direction of the program have been under W. P. Peck, High Temperature Materials Branch, Langley Research Center.

The authors wish to acknowledge the major contributions of A. J. Amaro, R. G. McKee, Jr., W. H. Johnson, and G. R. Plapp to the experimental program. The computer calculations were the work of Miss Margery Brothers.

CONTENTS

ABSTRACT ii

PREFACE iii

LIST OF ILLUSTRATIONS AND TABLES v

NOMENCLATURE vi

I INTRODUCTION 1

II THEORETICAL STUDIES 2

III EXPERIMENTAL STUDIES 11

A. Apparatus for Regression Rate Measurements 11

B. Regression Rate Measurements 13

C. Comparison with Calculated Weight Loss Behavior 25

IV CONCLUDING REMARKS 26

APPENDIX 27

COMPUTER CODE FOR CALCULATION OF HYBRID REGRESSION RATES . . 28

REFERENCES 37

ILLUSTRATIONS

1 Theoretical Weight Loss as a Function of Chamber Pressure (G_o^o = 0.05 lb/in.^{2}-sec) 4

2 Theoretical Weight Loss as a Function of Chamber Pressure (G_o^o = 0.10 lb/in.^{2}-sec) 5

3 Theoretical Weight Loss as a Function of Chamber Pressure (G_o^o = 0.15 lb/in.^{2}-sec) 6

4 Theoretical Weight Loss of a Pure Binder Hybrid Grain as a Function of Oxidizer Mass Flux 8

5 Theoretical Weight Loss of a Hybrid Grain Containing 20 Percent Aluminum as a Function of Oxidizer Mass Flux 9

6 Theoretical Weight Loss of a Hybrid Grain Containing 40 Percent Aluminum as a Function of Oxidizer Mass Flux 10

7 Oxygen Flow Control System. 12

8 Typical Weight Loss of a Hybrid Grain as a Function of Time . . 18

9 Experimental Weight Loss of Hybrid Grains as a Function of Chamber Pressure (G_o^o = 0.05 lb/in.^{2}-sec) 19

10 Experimental Weight Loss of Hybrid Grains as a Function of Chamber Pressure (G_o^o = 0.10 lb/in.^{2}-sec) 20

11 Experimental Weight Loss of Hybrid Grains as a Function of Chamber Pressure (G_o^o = 0.15 lb/in.^{2}-sec) 21

12 Experimental Weight Loss of a Pure Binder Hybrid Grain as a Function of Oxidizer Mass Flux 22

13 Experimental Weight Loss of a Hybrid Grain Containing 20 Percent Aluminum as a Function of Oxidizer Mass Flux 23

14 Experimental Weight Loss of a Hybrid Grain Containing 40 Percent Aluminum as a Function of Oxidizer Mass Flux 24

TABLES

1 Experimental Data Summary 14

NOMENCLATURE

B	Thermochemical mass transfer number
c_p	Specific heat at constant pressure
C	Constant
D_0	Initial diameter of grain
E_f	Gas-phase activation energy
G	Total mass flux
G_0^o	Oxidizer mass flux per unit area at $x = 0$ and $t = 0$
n	Order of the gas-phase reaction
L	Length of grain
p	Pressure
p_c	Chamber pressure
Q_f	Heat release per unit mass
$\dot{r}$	Regression rate
R	Gas constant
Re_x	Reynolds number based on x
t	Time
t_1	Characteristic time associated with combustion
T	Temperature; characteristic time associated with turbulent mixing
U_f	Flame temperature
U_w	Wall temperature

Subscripts

o	Conditions with zero surface mass injection; oxidizer
∞	Limiting value at high pressure

I. INTRODUCTION

Interest in the development of the hybrid rocket as an important propulsion device has naturally led to a consideration of its behavior over a wide range of operating chamber pressures. Early studies of hybrid combustion concentrated on the high-pressure regime in which the regression rate of the vaporizing surface is controlled by turbulent diffusion in the boundary layer, to the exclusion of any chemical kinetic effects.[1-6] The theory shows that in diffusion-limited combustion the regression rate is independent of pressure and depends only upon the mass flux through the port.

As the operating pressure is decreased, however, a pressure threshold is reached below which the chemical reaction time becomes significant compared to the mass diffusion time. In this regime of operation the regression rate becomes pressure-dependent at a fixed mass flux. Thus, the next step in the orderly development of hybrid combustion theory was the description of the behavior in the pressure-sensitive regime, which was carried out under a previous contract.[7] It was found that a relatively simple analytical model based on classical turbulent flame theory exhibited good agreement with the observed regression rate/pressure dependence at a single fixed oxidizer mass flux.

The current program was designed to supplement the previous investigation by obtaining data at two other oxidizer mass flux values for comparison with analytical predictions and to investigate the growth and decay of axial traveling waves produced by injecting pressure pulses from an explosive device. Only the regression measurements were carried out before cancellation of the contract after a decision was made by NASA to terminate their hybrid combustion research contracts. The data obtained corroborated the agreement between theory and experiment noted earlier.

II. THEORETICAL STUDIES

Theoretical studies carried out up to the time of the contract cancellation were concerned with improving the predictions of the model under conditions of varying mass flux. The initial analysis[7] gave good agreement with the regression rate/pressure behavior at constant oxidizer mass flux, but poor agreement with the regression rate/mass flux behavior at constant pressure. The problem has now been corrected by a reconsideration of the ratio of chemical reaction time to turbulent diffusion time in the boundary layer.

The regression rate $\dot{r}$ is given by the equation[2]

$$\frac{\dot{r}}{\dot{r}_\infty} = \left(\frac{2T}{t_1}\right)^{\frac{1}{2}} \left[1 - \frac{T}{t_1}\left(1 - e^{-t_1/T}\right)\right]^{\frac{1}{2}} \tag{1}$$

where $\dot{r}_\infty$ is the regression rate in the diffusion limit, t_1 is the characteristic chemical reaction time, and T is the characteristic turbulent diffusion time. Note that as $t_1/T \to 0$, $\dot{r}/\dot{r}_\infty \to 1$; i.e., when the reaction time is small compared to the diffusion time, the diffusion-controlled regression rate is recovered. The other limit, corresponding to $t_1/T \to \infty$, is

$$\frac{\dot{r}}{\dot{r}_\infty} = \left(\frac{2T}{t_1}\right)^{\frac{1}{2}} \tag{2}$$

In this limit, termed the kinetically controlled regime, the flame behaves as a premixed flame for which

$$\dot{r} = Cp^{n/2}\, U_f^{\;1+n/2}\, e^{-E_f/2RU_f} \left[1 - \frac{c_p(U_f - U_w)}{Q_f}\right]^{\frac{1}{2}} \tag{3}$$

It follows then that

$$\frac{t_1}{T} = C \frac{G^2 Re_x^{-0.4} B^{0.46}}{p^n U_f^{n+2} e^{-E_f/RU_f} \left[1 - \frac{c_p(U_f - U_w)}{Q_f}\right]} \qquad (4)$$

In the original formulation[7] the quantity ℓ_1/ℓ_2 appeared as a multiplier on the right-hand side of the equation. The distance ℓ_1 was the distance that the flame front propagates into unburned gas at the (kinetic) flame speed while ℓ_2 was the characteristic scale of turbulence. In this formulation t_1/τ was found to be proportional to the square root of the expression given in Eq. 4; this gave a dependence on mass flux G that did not agree with experimentally observed behavior. Much better qualitative agreement with the trends shown by the data is now obtained, as will be discussed in the next section.

To employ Eq. 4 it is necessary to choose a value for the empirical constant C. The empiricism enters the problem through the kinetics formulation in which the functional dependence of the reaction rate, but not its absolute value, is chosen. For the present calculations the constant was evaluated by assuming that $\dot{r}/\dot{r}_\infty = 0.75$ when p = 150 psia and $G_0^0 = 0.05/\text{in.}^2\text{-sec}$. These numerical choices are supported by the available experimental data that are given in the next section.

Calculations of weight loss as a function of chamber pressure for a 5-sec time interval are shown in Figs. 1 through 3. Weight loss is shown rather than regression rate because it is the measured quantity in the experiments. A print out of the computer code used for these calculations is given in the Appendix. Because the physical properties (density, heat of vaporization, flame temperature, etc.) of PU (polyurethane) and PBAN (polybutadiene-acrylic-nitrile) are nearly the same,[7] the computed weight losses for the two binder systems differed by no more than 2% over the ranges of pressure and oxidizer mass flux considered. Therefore, there is no differentiation between the two binder systems delineated in the figures. Oxygen was considered as the oxidizer in all of the calculations.

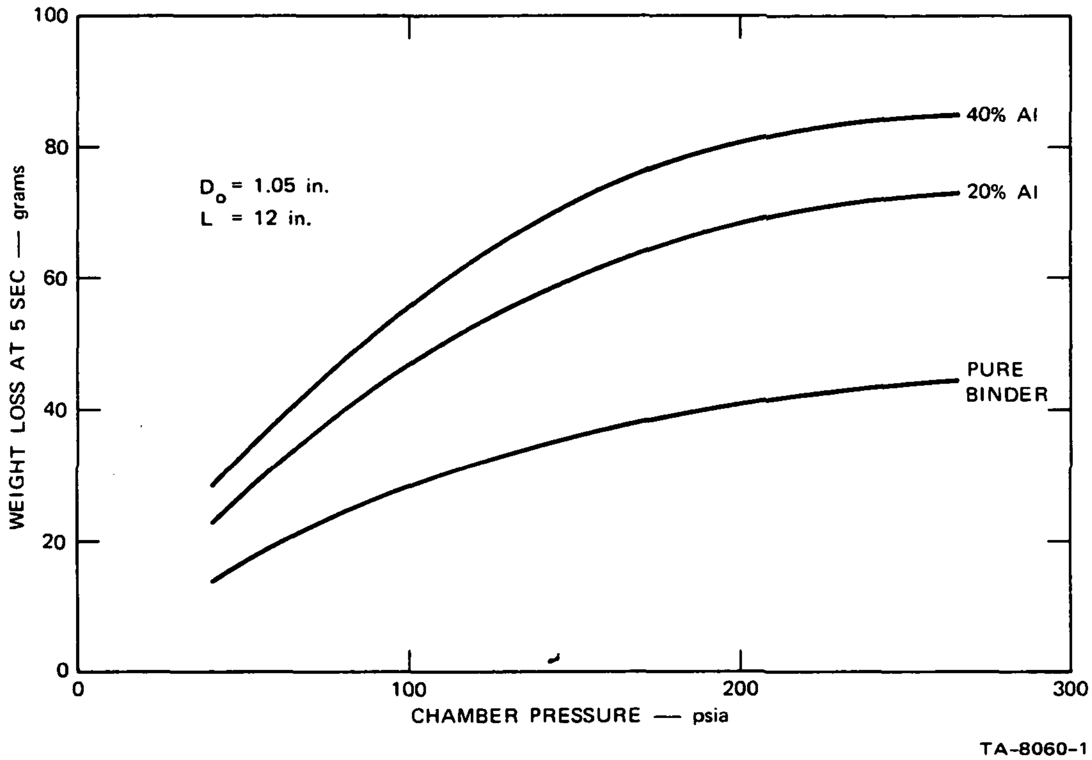

FIGURE 1 THEORETICAL WEIGHT LOSS AS A FUNCTION OF CHAMBER PRESSURE (G_o^o = 0.05 lb/in.^{2}-sec)

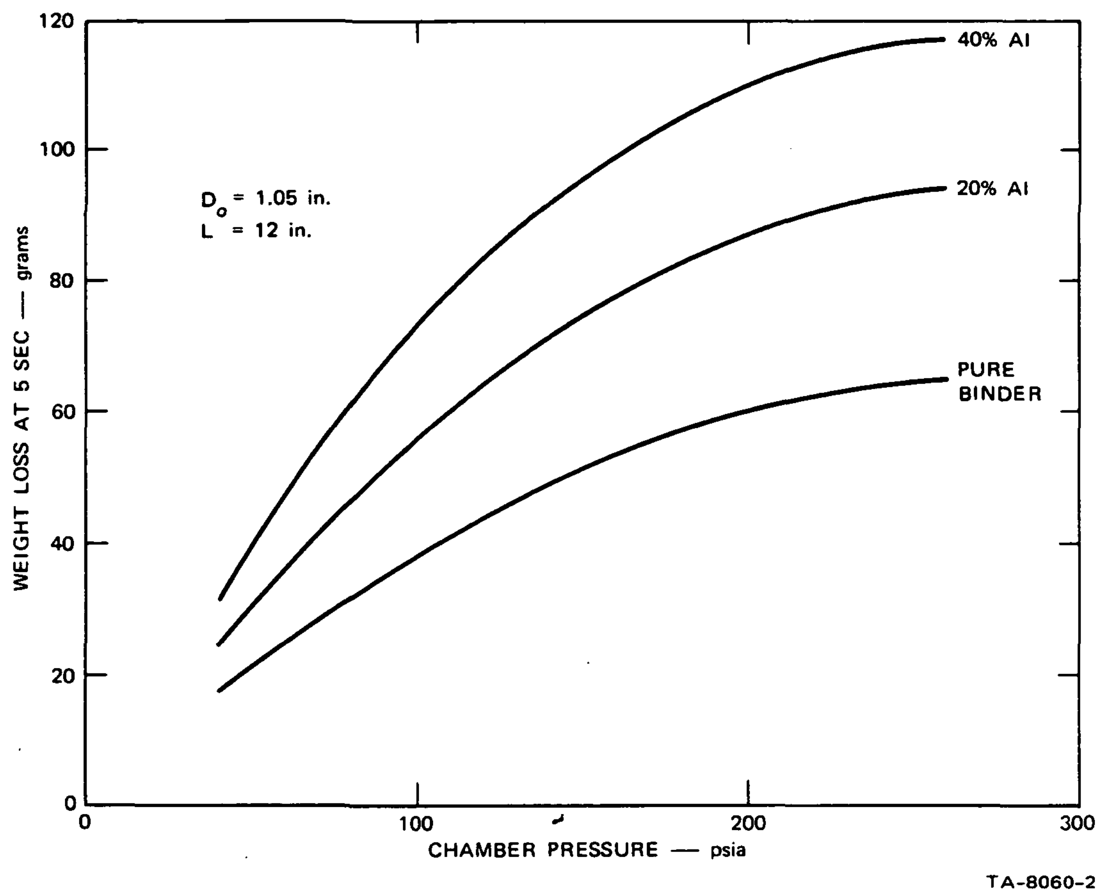

FIGURE 2 THEORETICAL WEIGHT LOSS AS A FUNCTION OF CHAMBER PRESSURE (G_o^o = 0.10 lb/in.^{2}-sec)

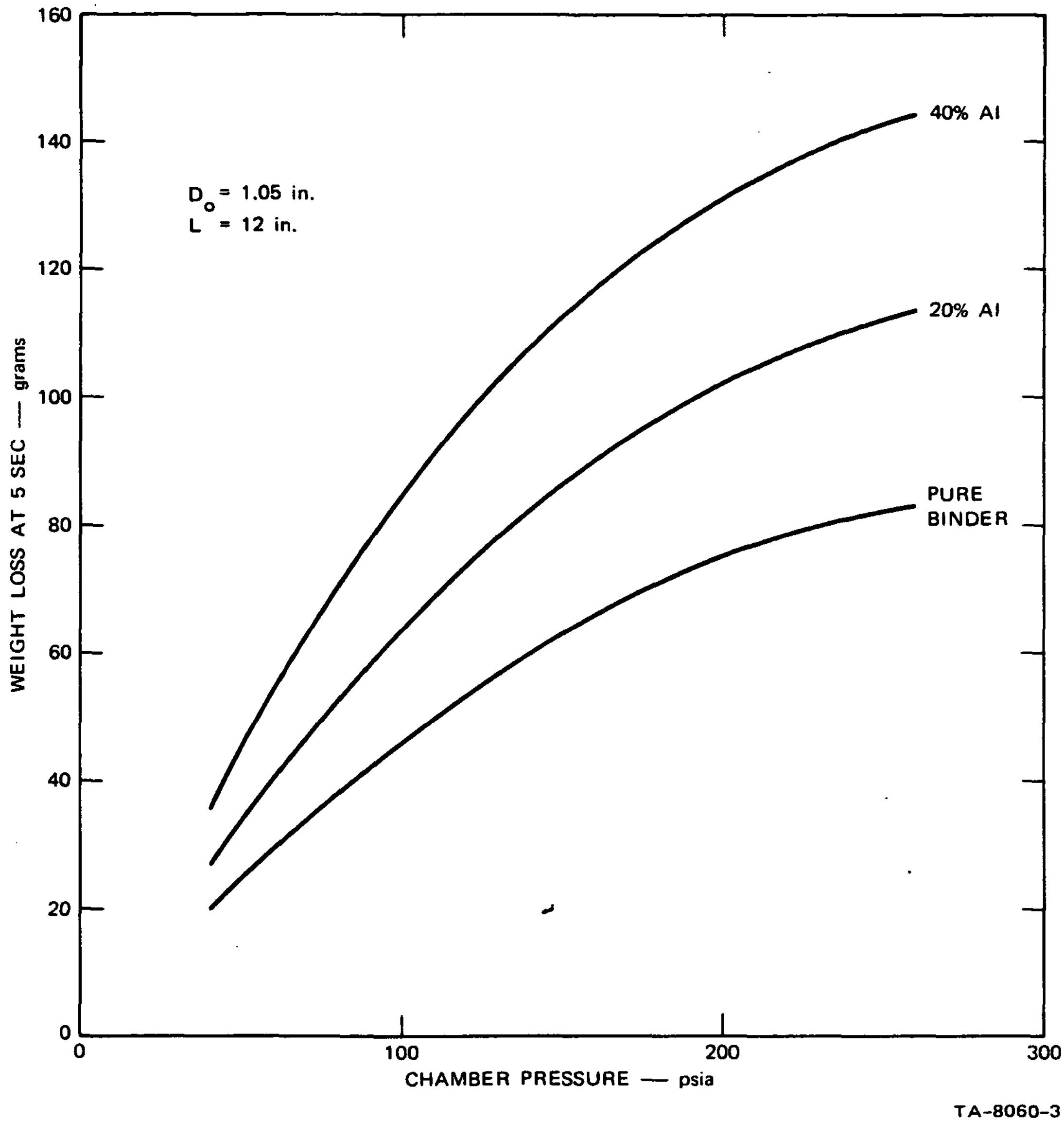

FIGURE 3 THEORETICAL WEIGHT LOSS AS A FUNCTION OF CHAMBER PRESSURE (G_o^o = 0.15 lb/in.^{2}-sec)

Figures 1 through 3 show that the dependence of weight loss on chamber pressure at low pressures becomes more marked as the oxidizer mass flux increases. Increasing the metal loading at a fixed oxidizer mass flux also amplifies the effect, in this case because of the dependence of radiative heat transfer on pressure.

Figures 4 through 6 are cross-plots of the results shown in Figs. 1 through 3 to show the dependence of weight loss on oxidizer mass flux as a function of chamber pressure. At low chamber pressures, in the kinetically controlled regime, the weight loss is nearly independent of oxidizer mass flux. As the pressure increases the slope of the curve increases, with the proportionality approaching something less than the 0.8 power. Here the diffusion-controlled regime, in which regression rate is proportional to the 0.8 power of the total mass flux, is being approached.

The trends predicted by the theory are, of course, those that were built in through the original formulation of the physical problem. The problem was formulated on the basis of past results obtained at SRI[7] and elsewhere.[8-10] A comparison with more recent data obtained under this contract is given in the next section.

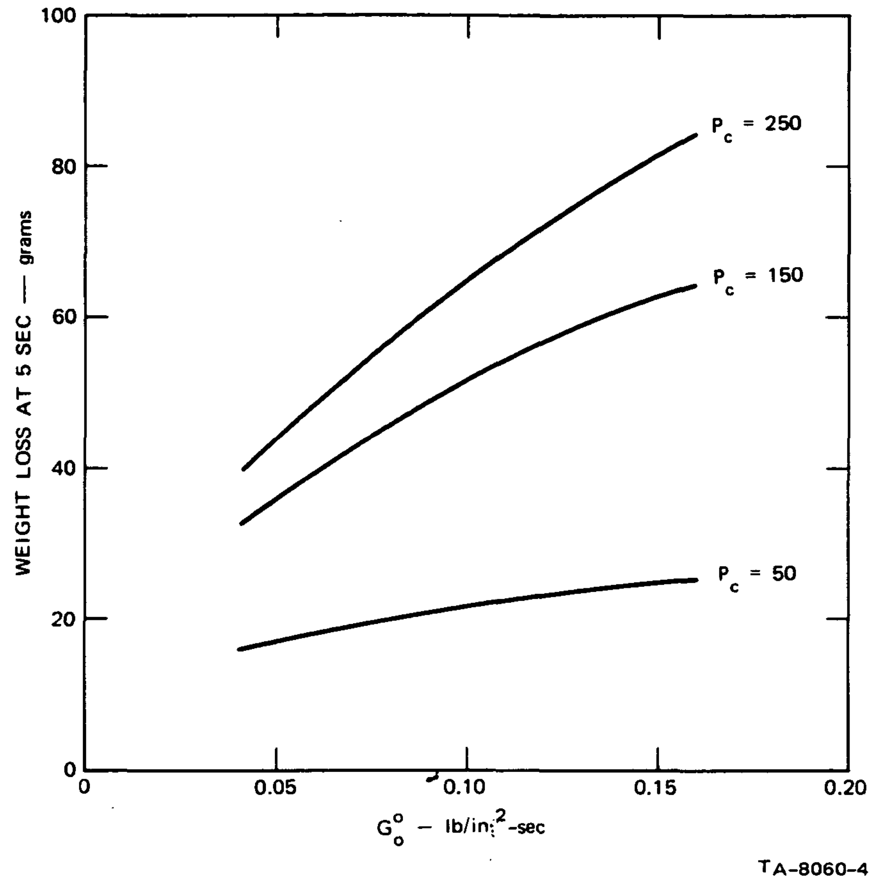

FIGURE 4 THEORETICAL WEIGHT LOSS OF A PURE BINDER HYBRID GRAIN AS A FUNCTION OF OXIDIZER MASS FLUX

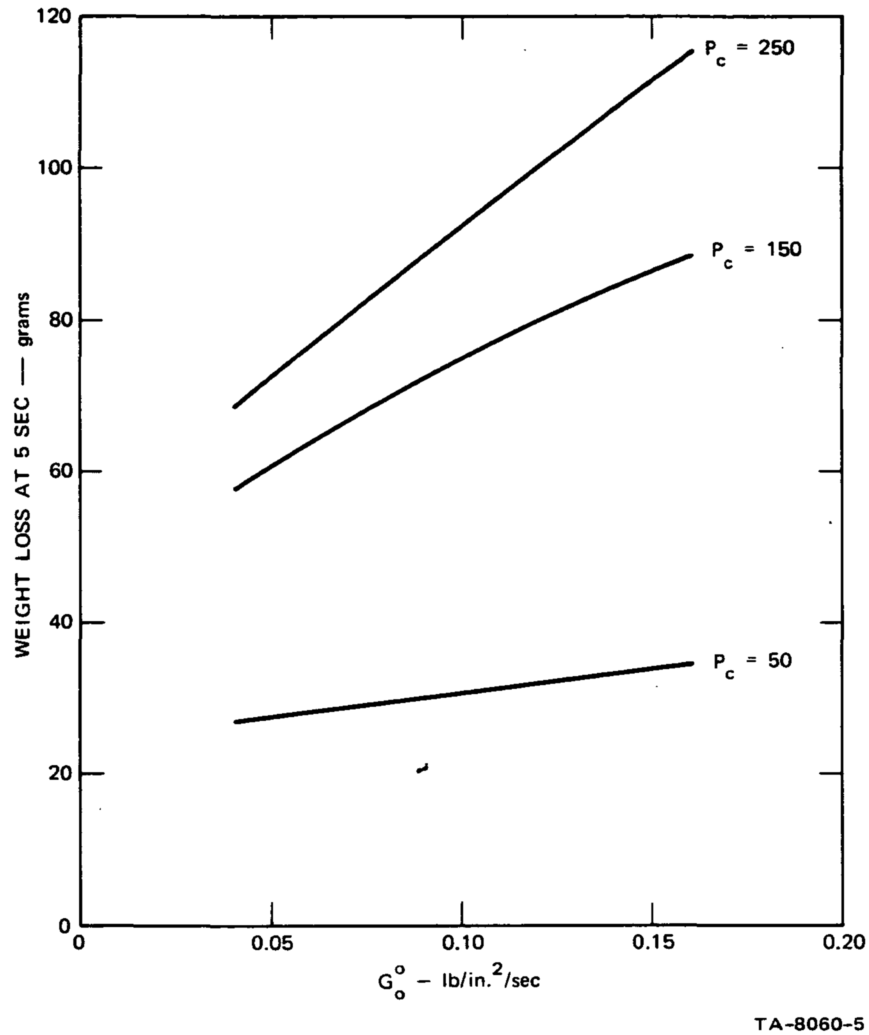

FIGURE 5 THEORETICAL WEIGHT LOSS OF A HYBRID GRAIN CONTAINING 20 PERCENT ALUMINUM AS A FUNCTION OF OXIDIZER MASS FLUX

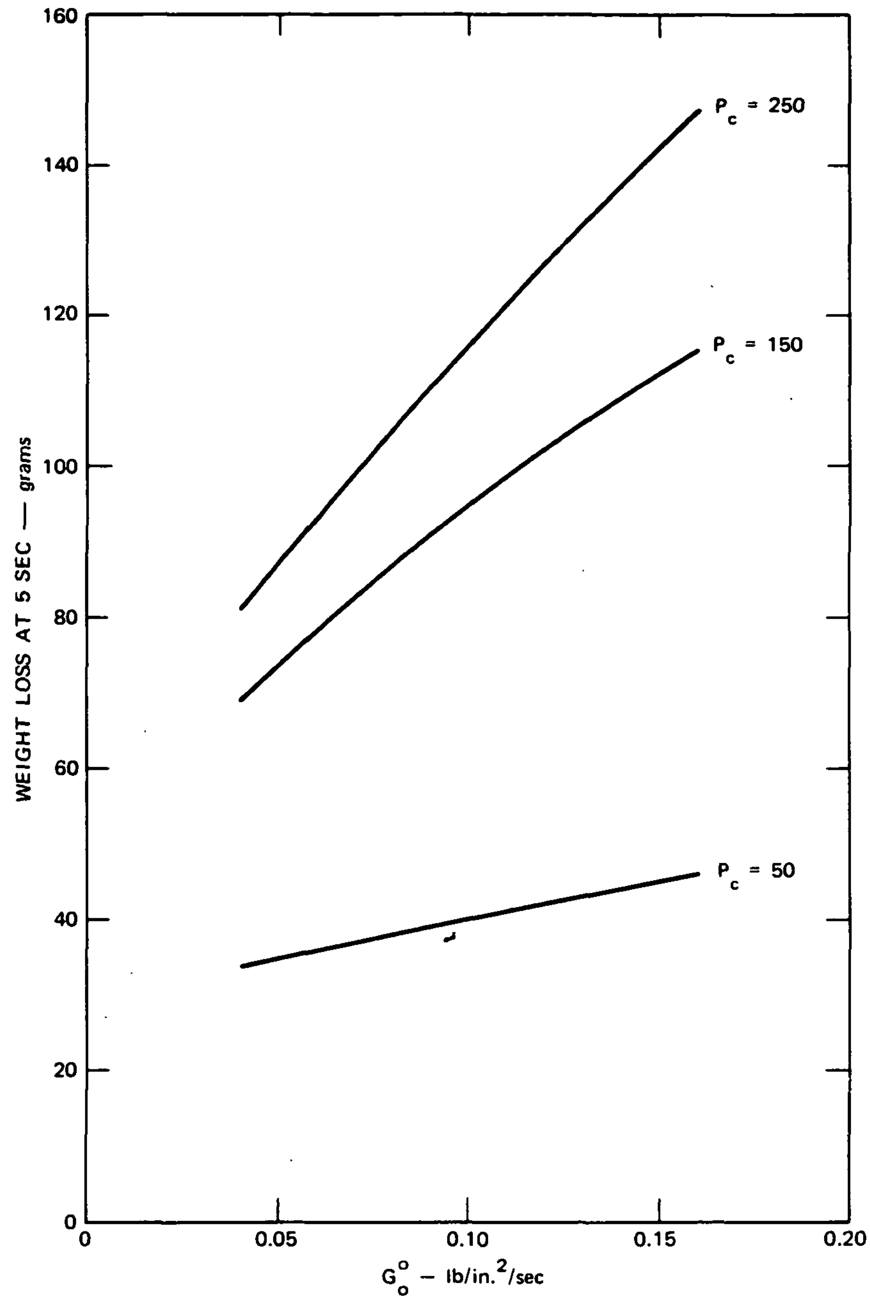

FIGURE 6 THEORETICAL WEIGHT LOSS OF A HYBRID GRAIN CONTAINING 40 PERCENT ALUMINUM AS A FUNCTION OF OXIDIZER MASS FLUX

III. EXPERIMENTAL STUDIES

The experimental studies were designed to provide data that would assist in the development of a theoretical model that could be used to predict the regression rate behavior and combustion instability limits for hybrid rocket motors operating in the low-pressure regime. The experiments originally proposed for this program included four types of tests:

1. Hybrid motor tests for determining the mean regression rate of various propellant systems in the pressure-sensitive regime over a range of oxidizer mass flux.
2. Hybrid motor tests in which axial instability would be induced by pressure pulses. The growth and decay of the pressure wave would be studied under varying operating conditions.
3. Slab burner tests to obtain Schlieren photographs of the relative thickness and position of the flame zone under the various operating conditions chosen.
4. Atmospheric combustion tests in the combustion simulator to determine the effect of heat release distribution on the heat transfer to the wall.

Because of the premature termination of the program only the first phase of the experimental studies was completed.

A. Apparatus for Regression Rate Measurements

The hybrid motor tests for determination of the mean regression rate utilized the existing flow facility that is shown schematically in Fig. 7. This facility was originally designed for liquid rocket engine tests with cryogenic oxidizers and was therefore constructed of 304 stainless steel with Teflon* and/or Kel-F† seats and seals. Sonic chokes operated above their critical pressure ratio were used to maintain a constant oxidizer mass flow throughout each test. These chokes were calibrated against a flow meter in the preceding hybrid combustion instability program (Contract No. NAS 1-7310).[7]

---

*Trademark, E. I. du Pont de Nemours and Co.
†Trademark, 3M Company

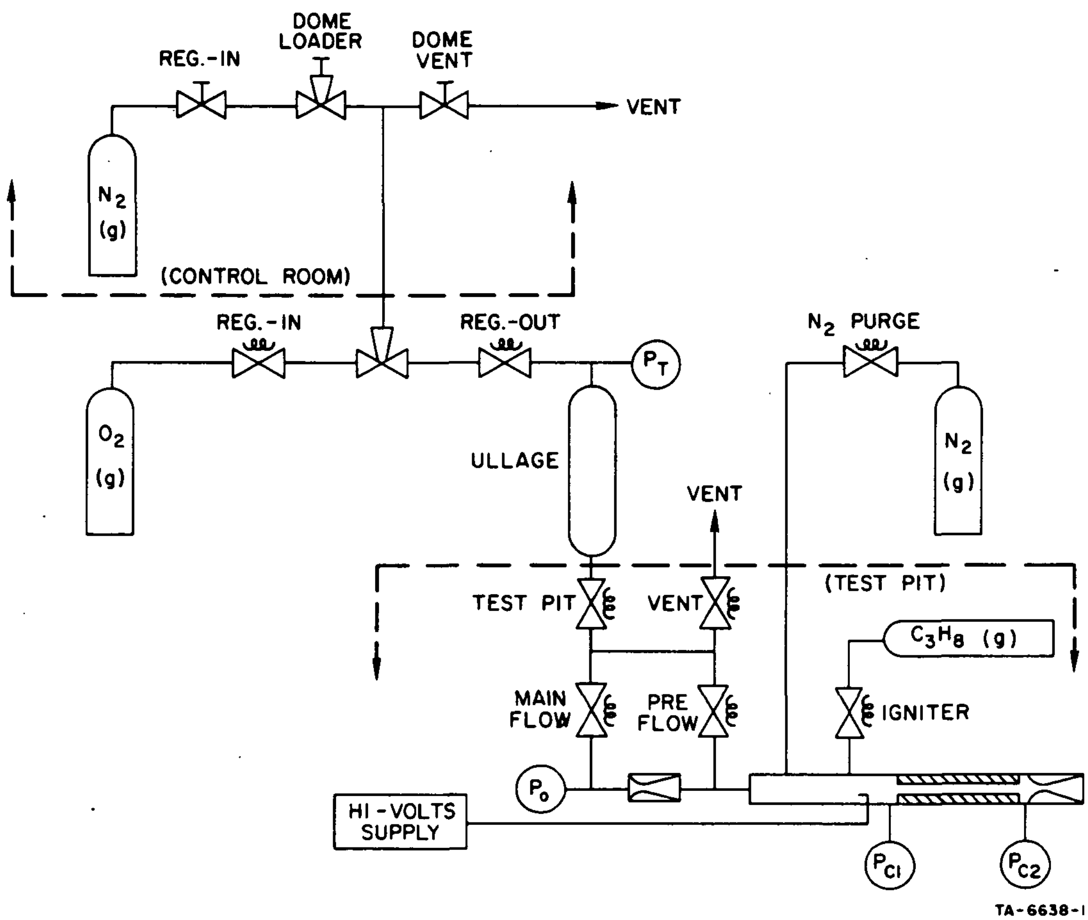

FIGURE 7 OXYGEN FLOW CONTROL SYSTEM

The motor configuration used was the same as in the prior program. The 2-1/2-inch-diameter motor consisted of a 12-inch flow-straightening section in which the ignition system was housed, a 12-inch tubular grain with a 1-inch-diameter internal perforation, and a water-cooled nozzle assembly.

The grain is ignited by preflowing a small amount of oxygen and propane into the chamber and igniting it with a spark plug. The ignition system is preset so that it operates near the lower flammability limit for the oxygen-propane mixture, thus yielding an oxygen-rich high-temperature source. The time for the flame to spread from the head end of the grain to the nozzle end was determined to be approximately 1 sec. Therefore, the main flow valve was delayed for that length of time. The weight of fuel typically consumed during this ignition process was determined to be 0.5 g which is about 1% of the amount of fuel that would be consumed in a 5-sec test at a regression rate of 0.01 in./sec.

B. <u>Regression Rate Measurements</u>

Weight loss data were obtained for test durations of both 5 and 10 seconds. The grains were dimensionally measured before and after each test. The data were obtained for PU and PBAN binders containing 0, 20, and 40 percent aluminum for chamber pressures ranging from 30 to 250 psia and for oxidizer mass fluxes of 0.05, 0.10, and 0.15 lb/in.^{2}-sec. The oxidizers used for all of the tests was gaseous oxygen. The data from these tests are presented in Table I. PU and PBAN were chosen for comparative binder tests because their surface behavior during regression is quite different. PU sublimes cleanly at the regressing surface after a melt is formed, while the regression of PBAN consists of the stripping of hydrogen from the surface layer, leaving a carbonaceous char that subsequently breaks away in particulate form.

Since these two systems behave differently the weight loss data will be subsequently discussed separately for each system; however, a brief discussion of the data handling procedure is in order.

Table I

EXPERIMENTAL DATA SUMMARY

Grain Number	Binder Type	Aluminum (%)	Chamber Pressure (psia)	G_o^o (lb/in.^{2}-sec)	Weight Loss (grams)	Run Duration (sec)
508	PU	0	34	0.05	45	5.1
509	PU	0	33	0.05	86	10.0
510	PU	0	77	0.05	58	5.0
511	PU	0	78	0.05	107	9.6
512	PU	0	165	0.05	77	5.0
513	PU	0	170	0.05	147	9.4
514	PU	0	260	0.05	79	4.0
515	PU	0	253	0.05	156	9.2
527	PU	0	75	0.10	59	5.0
528	PU	0	260	0.10	97	5.0
517	PU	0	35	0.15	60	5.0
518	PU	0	35	0.15	108	9.6
519	PU	0	80	0.15	67	5.0
521	PU	0	74	0.15	124	9.6
523	PU	0	160	0.15	87	4.9
524	PU	0	130	0.15	163	9.6
525	PU	0	225	0.15	92	4.9
526	PU	0	230	0.15	202	9.6
556	PU	20	34	0.05	49	4.7
557	PU	20	35	0.05	101	9.5
558	PU	20	72	0.05	60	5.0
559	PU	20	81	0.05	133	9.8
560	PU	20	130	0.05	82	5.0
561	PU	20	138	0.05	174	9.6
543	PU	20	36	0.10	59	5.0
544	PU	20	35	0.10	128	9.8
545	PU	20	71	0.10	84	5.0
546	PU	20	87	0.10	186	9.8
547	PU	20	156	0.10	130	5.0
548	PU	20	163	0.10	252	9.8
549	PU	20	32	0.15	65	5.2
550	PU	20	35	0.15	128	9.7
551	PU	20	62	0.15	82	5.0
552	PU	20	83	0.15	196	9.8
553	PU	20	157	0.15	139	5.1
554	PU	20	169	0.15	277	9.5

Table I (contd)

Grain Number	Binder Type	Aluminum (%)	Chamber Pressure (psia)	G_o^o (lb/in.^{2}-sec)	Weight Loss (grams)	Run Duration (sec)
445	PU	40	34	0.05	51	4.8
446	PU	40	42	0.05	139	9.4
447	PU	40	103	0.05	116	4.8
448	PU	40	37	0.10	70	4.6
449	PU	40	36	0.10	141	9.6
451	PU	40	75	0.10	100	5.0
565	PU	40	65	0.10	201	9.4
452	PU	40	183	0.10	178	5.0
566	PU	40	177	0.10	174	4.8
567	PU	40	170	0.10	362	9.4
438	PU	40	35	0.15	76	4.8
439	PU	40	37	0.15	164	9.5
440	PU	40	67	0.15	97	4.8
441	PU	40	67	0.15	232	9.8
442	PU	40	153	0.15	186	5.0
443	PU	40	158	0.15	396	9.6
209	PBAN	0	32	0.05	56	5.0
211	PBAN	0	32	0.05	105	10.0
201	PBAN	0	85	0.05	74	4.0
204	PBAN	0	85	0.05	157	10.1
207	PBAN	0	160	0.05	85	5.2
208	PBAN	0	158	0.05	148	10.0
212	PBAN	0	235	0.05	75	5.1
213	PBAN	0	220	0.05	123	9.4
498	PBAN	0	32	0.10	55	5.3
505	PBAN	0	35	0.10	112	9.7
500	PBAN	0	80	0.10	84	5.4
501	PBAN	0	80	0.10	158	9.9
499	PBAN	0	170	0.10	94	5.3
504	PBAN	0	175	0.10	174	9.8
502	PBAN	0	225	0.10	92	5.2
503	PBAN	0	225	0.10	166	9.8
199	PBAN	0	31	0.15	52	4.8
200	PBAN	0	30	0.15	98	9.5
197	PBAN	0	74	0.15	75	4.8
198	PBAN	0	74	0.15	152	9.4
169	PBAN	0	157	0.15	98	5.0
192	PBAN	0	158	0.15	188	9.6

Table I (concld)

Grain Number	Binder Type	Aluminum (%)	Chamber Pressure (psia)	G_0^0 (lb/in.^{2}-sec)	Weight Loss (grams)	Run Duration (sec)
268	PBAN	20	32	0.05	70	5.1
269	PBAN	20	31	0.05	122	10.0
272	PBAN	20	75	0.05	88	5.3
273	PBAN	20	75	0.05	162	9.6
270	PBAN	20	150	0.05	101	5.2
271	PBAN	20	158	0.05	172	10.0
274	PBAN	20	220	0.05	87	5.0
275	PBAN	20	210	0.05	143	9.6
477	PBAN	20	32	0.10	56	5.2
478	PBAN	20	32	0.10	122	9.6
479	PBAN	20	77	0.10	94	5.3
480	PBAN	20	80	0.10	177	9.8
481	PBAN	20	145	0.10	108	5.3
482	PBAN	20	149	0.10	199	9.8
483	PBAN	20	230	0.10	111	5.3
484	PBAN	20	236	0.10	187	9.8
260	PBAN	20	31	0.15	65	4.9
263	PBAN	20	31	0.15	128	9.6
258	PBAN	20	67	0.15	91	4.8
259	PBAN	20	70	0.15	184	9.5
256	PBAN	20	150	0.15	119	4.8
257	PBAN	20	145	0.15	242	9.6
456	PBAN	40	30	0.05	62	5.2
457	PBAN	40	30	0.05	120	9.6
458	PBAN	40	75	0.05	95	5.2
460	PBAN	40	75	0.05	189	9.6
461	PBAN	40	150	0.05	111	4.9
462	PBAN	40	155	0.05	198	9.6
470	PBAN	40	35	0.10	74	5.2
471	PBAN	40	39	0.10	153	9.6
468	PBAN	40	78	0.10	112	5.2
469	PBAN	40	85	0.10	219	9.8
466	PBAN	40	160	0.10	132	5.2
467	PBAN	40	167	0.10	252	9.6
323	PBAN	40	30	0.15	73	4.9
324	PBAN	40	31	0.15	138	9.4
320	PBAN	40	71	0.15	100	4.9
321	PBAN	40	78	0.15	215	9.6
318	PBAN	40	147	0.15	145	4.8
319	PBAN	40	155	0.15	315	9.6

Typical weight loss data as a function of time are presented in Fig. 8. The mean chamber pressure at which the fuel is burnt is denoted beside each data point. Since minor variations in test duration did occur, the data were standardized at 5 sec. This relatively short time was chosen to minimize the effect of the change in oxidizer mass flux as the internal perforation diameter increased. The data were then plotted as a function of chamber pressure and oxidizer mass flux for the various aluminum loadings made. From the weight loss versus chamber pressure curves, constant pressure lines were constructed for the weight loss verus oxidizer mass flux curves. The chamber pressure values used are mean values. For either pure PBAN or PU the observed pressure deviation about the mean was very minor. However, in the systems that contained aluminum the deviations were much more severe because of the coating of the nozzle throat with aluminum oxide. The most severe cases were those in which the chamber pressure was high and/or the oxidizer mass flux was low; both cases necessitate small nozzle throat sizes. With this variation a precise mean value of chamber pressure for repetitive tests were difficult to obtain.

Under the current program the first data to be taken were the weight loss data at the low value of oxidizer mass flux. These data are presented in Fig. 9. Upon examining the data, it can be seen that the PBAN results fall off for chamber pressures above 150. One possible explanation is that this decline occurs when the velocity is reduced below the level required to efficiently remove the char layer that is present. This idea is supported by the results shown in Fig. 10 where the oxidizer mass flux is 0.10 lb/in.^{2}-sec. Here the velocity is large enough to stabilize the regression rate for pressures over 150. In Fig. 11 the oxidizer mass flux is further increased and the regression rate becomes a function of chamber pressure throughout the range of test conditions.

The dependency of weight loss of the PBAN system on oxidizer mass flux is depicted in Figs. 12 through 14. At lower values of chamber pressure the regression rate is relatively independent of mass flux. However, as the chamber pressure is increased the transition from a kinetically

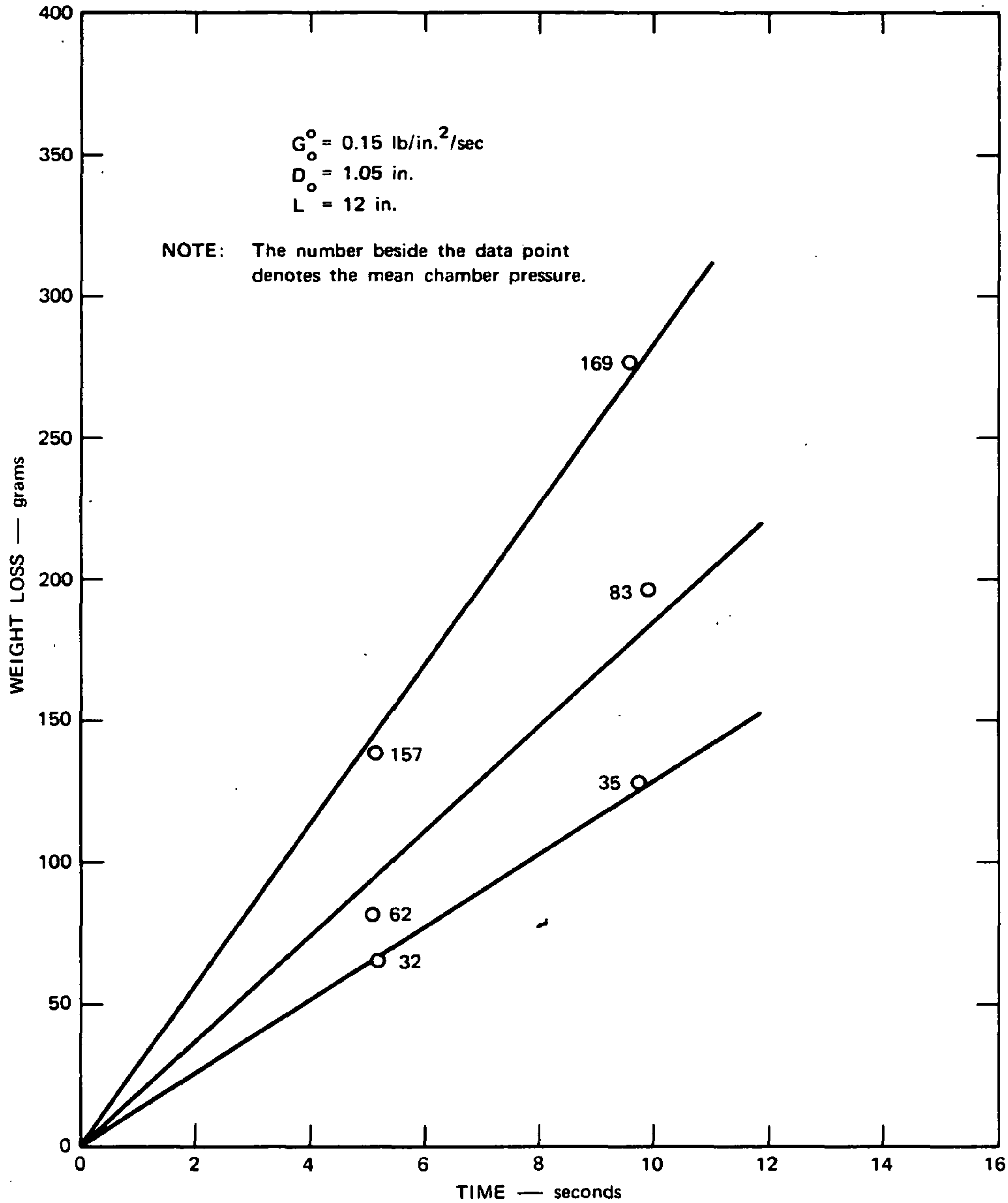

TA-8060-13

FIGURE 8 TYPICAL WEIGHT LOSS OF A HYBRID GRAIN AS A FUNCTION OF TIME

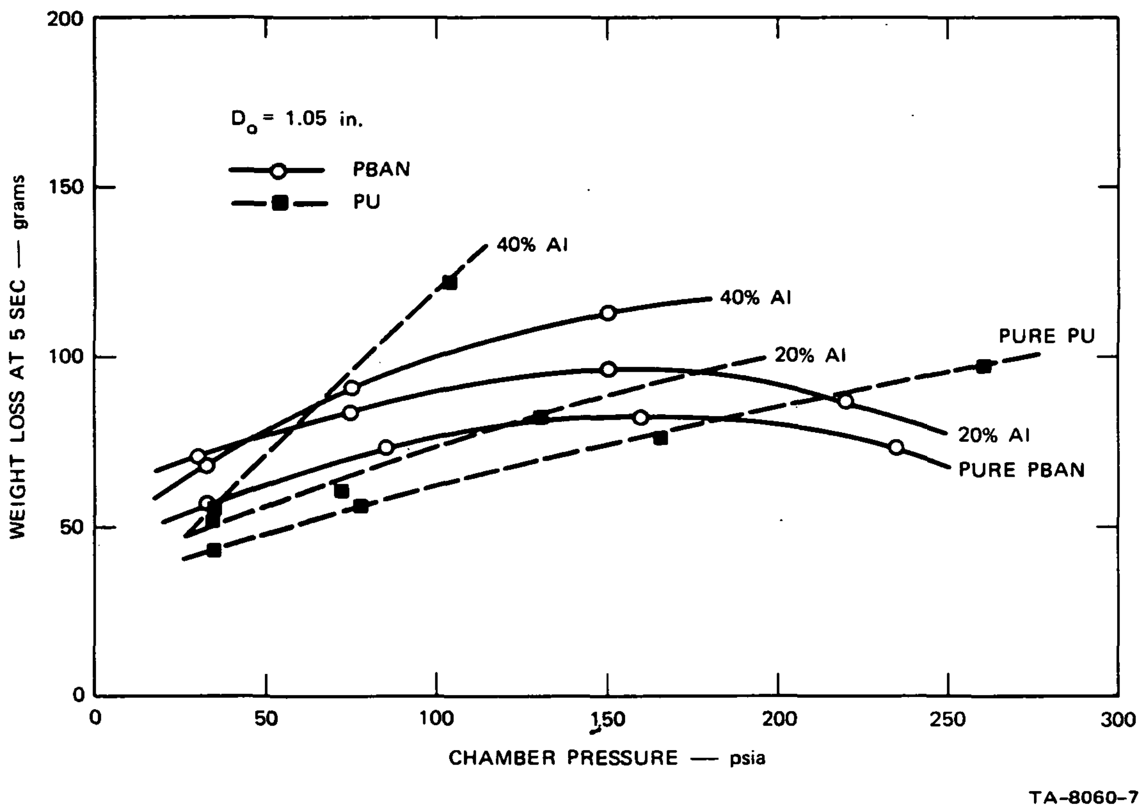

FIGURE 9 EXPERIMENTAL WEIGHT LOSS OF HYBRID GRAINS AS A FUNCTION OF CHAMBER PRESSURE (G_o^o = 0.05 lb/in.^{2}-sec)

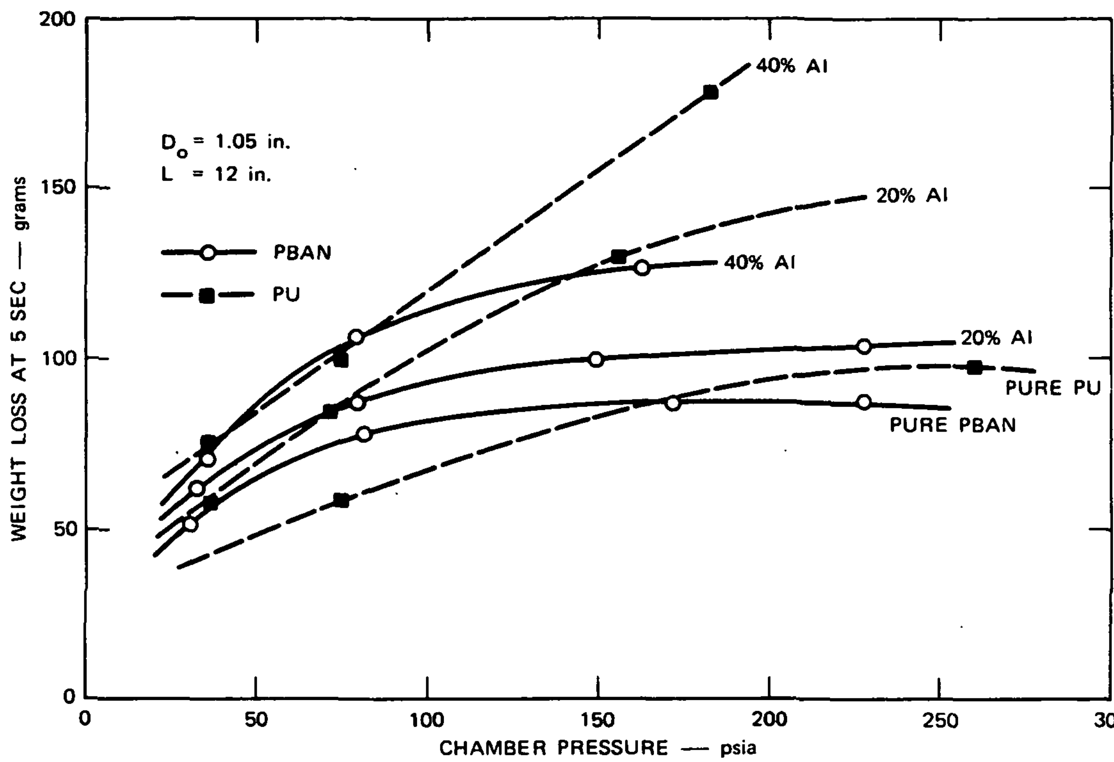

TA-8060-8

FIGURE 10 EXPERIMENTAL WEIGHT LOSS OF HYBRID GRAINS AS A FUNCTION OF CHAMBER PRESSURE (G_o^o = 0.10 lb/in.^{2}-sec)

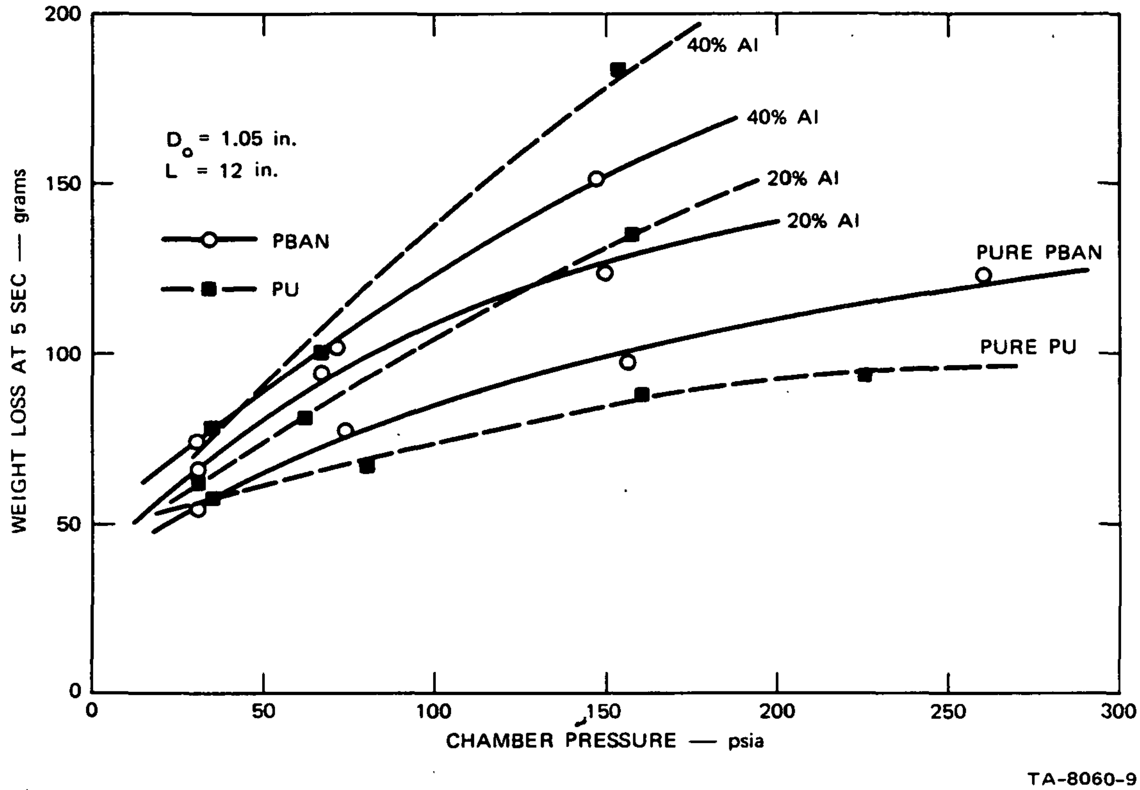

FIGURE 11 EXPERIMENTAL WEIGHT LOSS OF HYBRID GRAINS AS A FUNCTION OF CHAMBER PRESSURE (G_o^o = 0.15 lb/in.^{2}-sec)

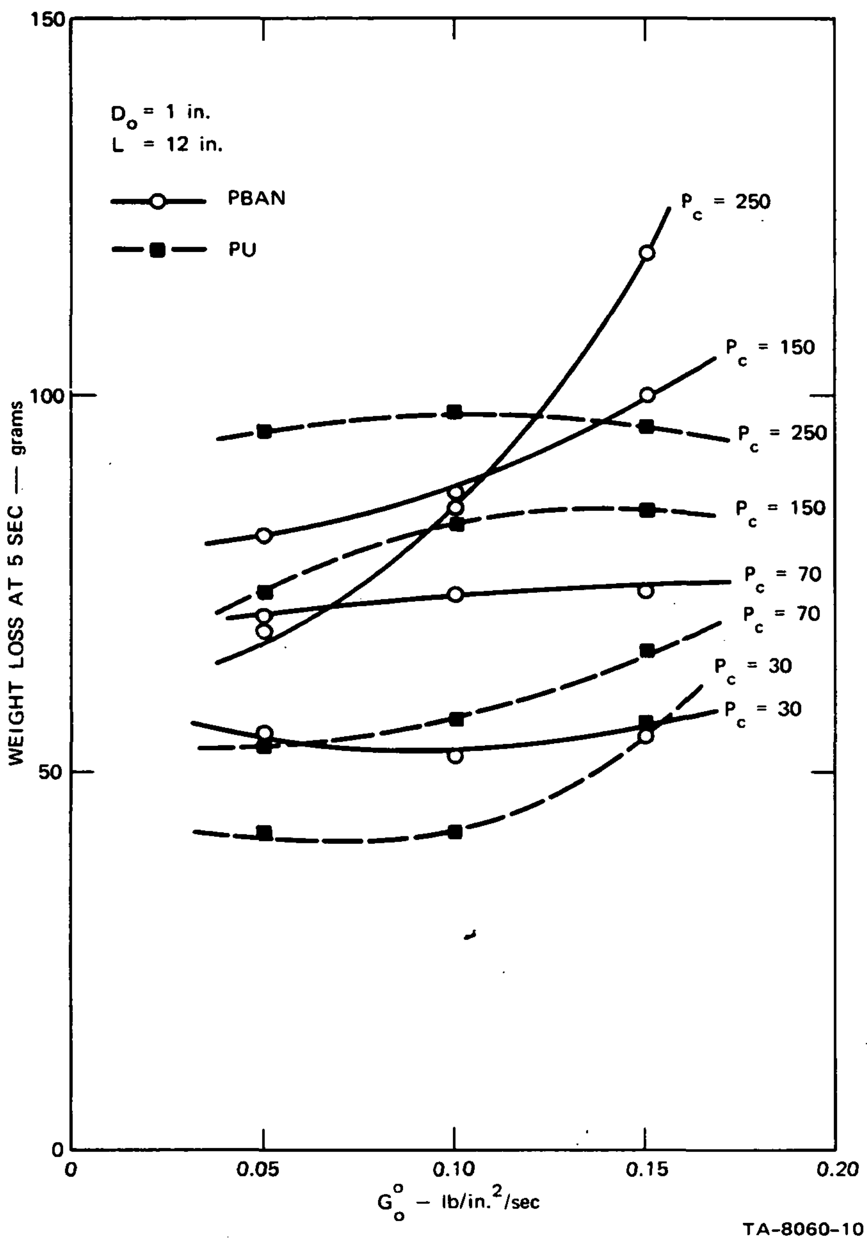

FIGURE 12 EXPERIMENTAL WEIGHT LOSS OF A PURE BINDER HYBRID GRAIN AS A FUNCTION OF OXIDIZER MASS FLUX

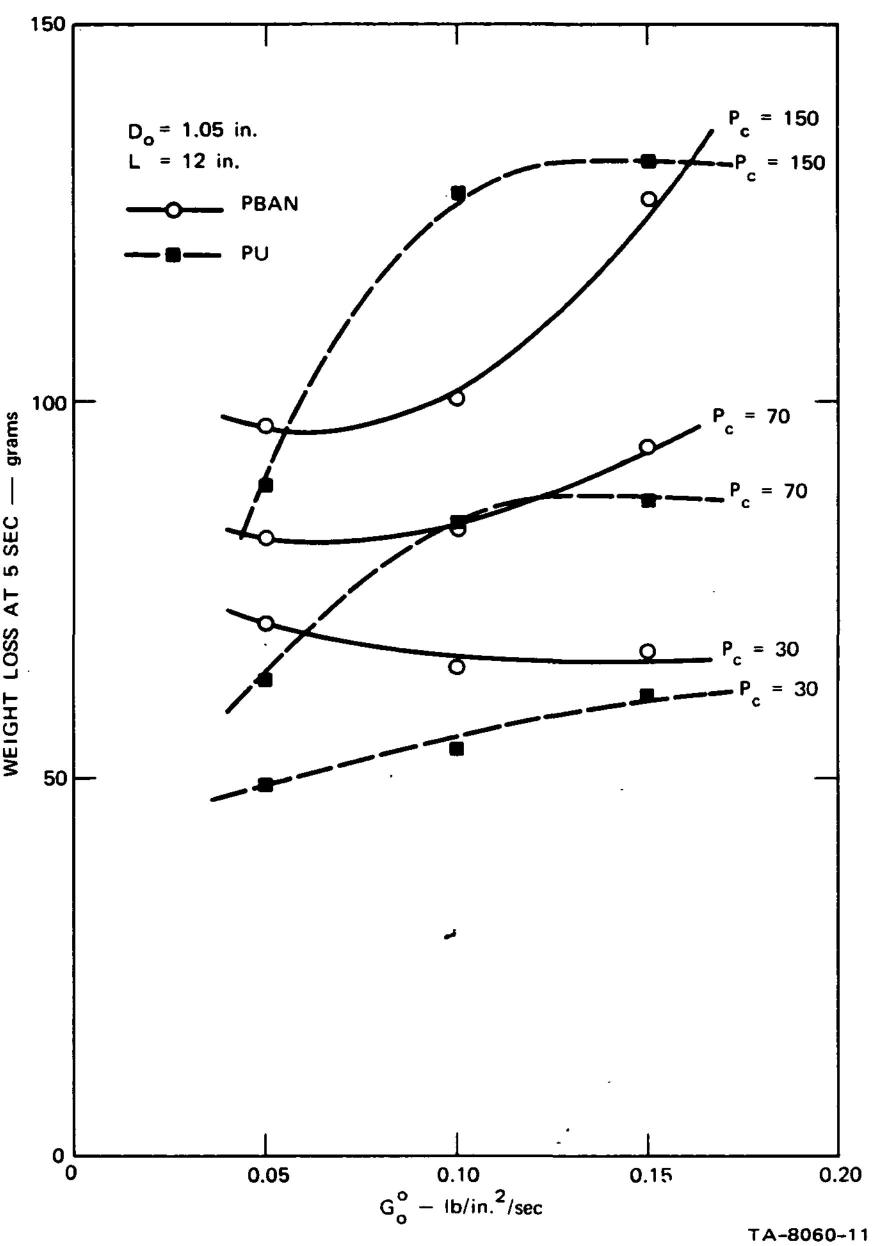

FIGURE 13 EXPERIMENTAL WEIGHT LOSS OF A HYBRID GRAIN CONTAINING 20 PERCENT ALUMINUM AS A FUNCTION OF OXIDIZER MASS FLUX

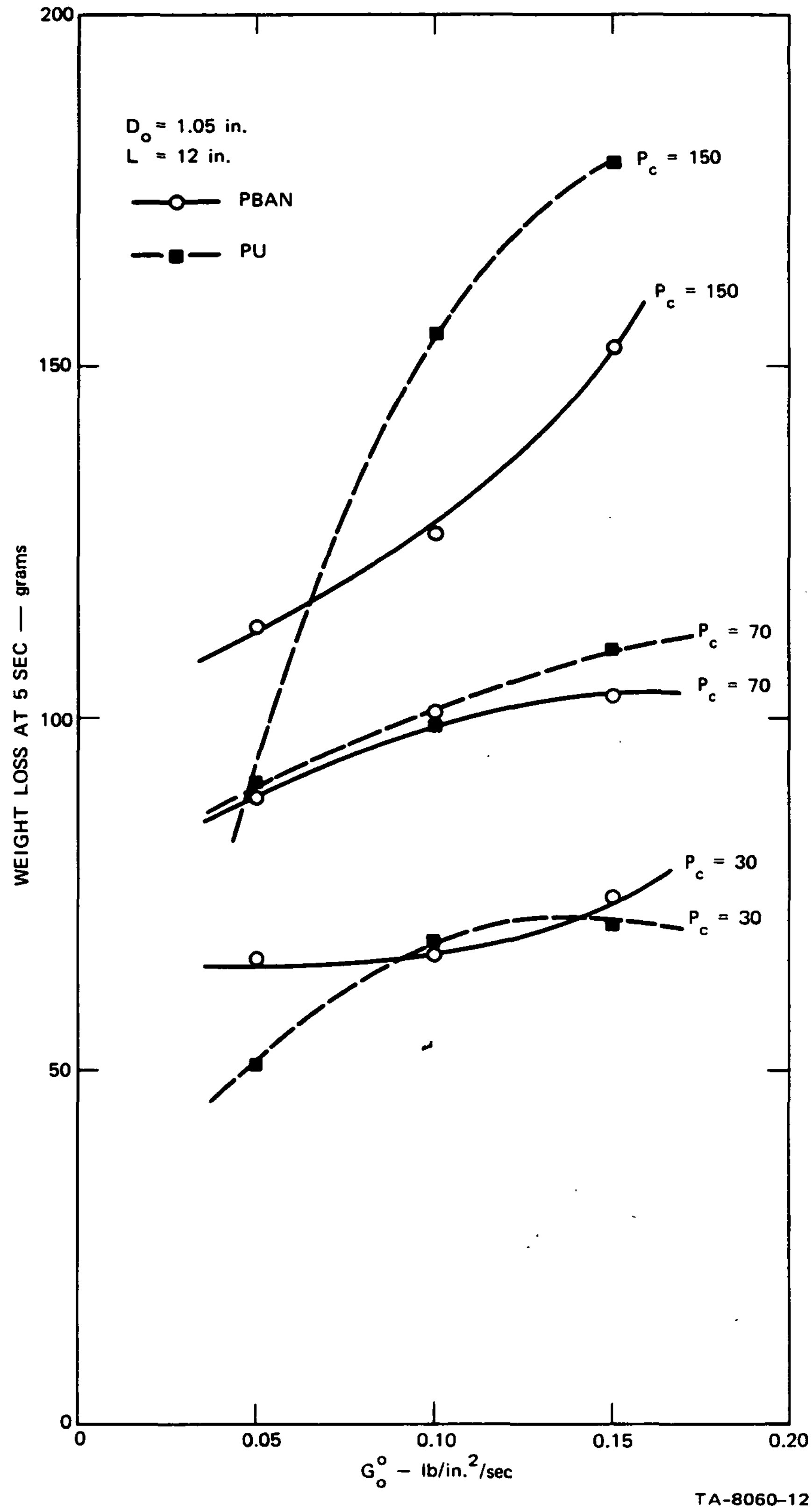

FIGURE 14 EXPERIMENTAL WEIGHT LOSS OF A HYBRID GRAIN CONTAINING 40 PERCENT ALUMINUM AS A FUNCTION OF OXIDIZER MASS FLUX

controlled regression rate to a diffusion-limited process is apparent.

As mentioned previously the PU system exhibits a different combustion mechanism than the PBAN system. As can be seen from the weight loss versus chamber pressure data which are also shown in Figs. 9 through 11, the PU system's regression rate is dependent upon chamber pressure for all of the values of oxidizer mass flux investigated. Since this system melts rather than chars, the velocity effect at constant oxidizer mass flux is absent. However, the influence of velocity is noticeable at low chamber pressures and high oxidizer mass flux. This is thought to be an erosion effect which is diminished by the addition of the aluminum. The aluminum not only increases the viscosity of the melted surface layer but also reduces the thermal profile thickness by increasing the regression rate.

C. Comparison with Calculated Weight Loss Behavior

A comparison between Figs. 1 through 3 and Figs. 9 through 11 shows that the qualitative behavior of weight loss as a function of chamber pressure is in best agreement with the calculated behavior at the highest oxidizer mass flux. At the lowest value of mass flux the PBAN curves tend to droop at high pressure, presumably because the velocity is too low to remove the char layer, and the PU curves tend to rise at low pressure, presumably because of erosive effects on the melted binder surface at low pressure. This behavior is also reflected in a comparison of Figs. 4 through 6 with Figs. 12 through 14.

In all cases the measured weight loss is larger than the predicted value. The reason for this discrepancy was not known at the time work was halted on the contract.

IV. CONCLUDING REMARKS

A simple analysis to describe the transition of hybrid rocket combustion from the diffusion-limited region at high pressure to the kinetic limited domain at low pressure has been developed. Good qualitative agreement has been obtained with measured regression rate behavior in those operating regimes where surface effects such as excessive melting or charring do not occur.

It remains to be seen whether the simple model can describe instability behavior in the pressure-sensitive regime. Future investigations of hybrid combustion phenomena should be directed toward an understanding of this regime of operation.

Appendix

COMPUTER CODE FOR CALCULATION OF HYBRID REGRESSION RATES

```
                    PROGRAM HYBRID(INPUT,OUTPUT,TAPE5=INPUT,TAPE6=OUTPUT)
000003              REAL L,K,K1,K2,K3,K4,K5,K8,K9,M,M0,M1,M2,M3,N(100),NN,MR
000003              DIMENSION D(100),DATE(12),FUEL(12),OXID(12)
              C     THIS PROGRAM IS BASED UPON HEAT-TRANSFER LIMITED HYBRID THEORY.
              C     IT CALCULATES THE REGRESSION BEHAVIOR OF A CIRCULAR TUBE FUEL
              C     GRAIN.  THE INPUTS WHICH ARE NECESSARY FOR OPERATION OF THE
              C     PROGRAM ARE DEFINED AS FOLLOWS:
              C         D0 IS INITIAL INNER DIAMETER (IN.)
              C         L IS LENGTH (IN.)
              C         D2 IS OUTER DIAMETER (IN.)
              C         K IS MASS FRACTION OF NON-VOLATILE SURFACE MATERIAL
              C         K1 IS MASS FRACTION OF VOLATILE SURFACE MATERIAL WHICH FORMS
              C         PARTICULATE COMBUSTION PRODUCTS
              C         K2 IS TOTAL DENSITY OF FUEL GRAIN (LB/IN**3)
              C         K3 IS EFFECTIVE HEAT OF GASIFICATION (BTU/LB)
              C         M0 IS OXIDIZER FLOW RATE (LB/SEC)
              C             (IF M0 VARIES, IT MAY EITHER BE READ AS DATA OR
              C              DESCRIBED BY AN EQUATION.)
              C         P0 IS CHAMBER PRESSURE (PSIA)  (SEE THE ABOVE)
              C         J IS CASE NUMBER
              C             J=1 IF PARTICLES IN THE GRAIN PRODUCE PARTICULATE
              C             COMBUSTION PRODUCTS
              C             J=2 IF PARTICLES IN THE GRAIN PRODUCE GASEOUS
              C             COMBUSTION PRODUCTS
              C             J=3 IF A COMPLETELY VOLATILE GRAIN PRODUCES PARTICULATE
              C             COMBUSTION PRODUCTS
              C         U0 IS OXIDIZER TEMP. AT INLET (DEG RANKINE)
              C         U5 IS COMBUSTION TEMP. AT AN O/F RATIO WHICH IS 3/4 OF THE
              C         STOICHIOMETRIC VALUE AT 5 ATM. PRESSURE (DEG RANKINE)
              C         C7 IS GAS-PHASE RADIATION CONSTANT
              C         K4 IS MASS OF OXIDIZER CONSUMED PER UNIT MASS OF NON-VOLATILE
              C         SURFACE MATERIAL IN PRODUCING PARTICULATE COMBUSTION PRODUCTS
              C         K5 IS MASS OF OXIDIZER CONSUMED PER UNIT MASS OF VOLATILE
              C         SURFACE MATERIAL IN PRODUCING PARTICULATE COMBUSTION PRODUCTS
              C         C8 IS MASS OF PARTICULATE COMBUSTION PRODUCTS FORMED PER UNIT
              C         MASS OF NON-VOLATILE SURFACE MATERIAL
              C         E2 IS EMISSIVITY (ABSORPTIVITY) OF FUEL SURFACE
              C         B IS MASS TRANSFER NUMBER
              C         K8 IS DENSITY OF PARTICULATE COMBUSTION PRODUCTS (LB/IN**3)
              C         C2 IS BOUNDARY LAYER DENSITY CORRECTION FACTOR
              C         S IS OXIDIZER VISCOSITY AT TEMP. U0 (LB/IN-SEC)
              C         T1 IS TIME INCREMENT FOR CALCULATIONS (SEC)
              C         T2 IS QUIT TIME (SEC)
              C         T3 IS TIME INCREMENT FOR PRINTOUT (SEC)
              C         X1 IS DISTANCE INCREMENT FOR CALCULATIONS (X/L)
              C         C9 IS THE RADIATION TEMPERATURE CONSTANT
              C         R6 IS THE PARTICLE RADIUS IN MICRONS
000003              READ(5,1000) (DATE(I),I=1,12)
000015         1000 FORMAT(12A6)
000015           10 READ(5,1010) D0,L,D2,K,K1,K2,K3,K4,K5,C8,C9,T1,T2,T3,
                   1             M0,P0,U0,U5,E2,B,K8,R6,QF
000077              IF(D0.EQ.0.0)GO TO 850
000100         1010 FORMAT(7F10.4)
000100              READ(5,1020) J
000106         1020 FORMAT(I1)
000106              READ(5,1000) (FUEL(I),I=1,12)
000120              READ(5,1000) (OXID(I),I=1,12)
```

```
000132        E3=0.0                                                          056
000133        U2=U5*(1.0+3.33E-4*(P0-75.0))                                   057
000140        C7=0.003                                                        059
000141        CP=0.4
000143        NN=2.0
000144        EF=27000.0
000146        RR=0.75
000147        TER=2.0
000151   3000 TEX=2.0*TER-RR**2*TER**2+2.0*EXP(-TER)
000162        IF(TEX.LT.2.01)GO TO 3020
000165        TER=TER+0.01
000167        GO TO 3000
000167   3010 TER=TER-0.01
000171        GO TO 3000
000172   3020 IF(TEX.LT.1.99)GO TO 3010
000175        WRITE(6,2070)TER
000202        MR=0.0433
000203        AR=0.8659
000205        PR=150.0
000206        UWR=1440.0
000210        UFR=U5*(1.0+3.33E-4*(PR-75.0))
000215        E1=3.307E-15                                                    060
000216        C6=(3.0*16.387E12)/(4.0*K8*R6**3)
000222        J1=1                                                            063
000223        C1=0.036                                                        064
000225        C2=1.0                                                          065
000226        S=3.00E-6                                                       066
000230        C3=(S/L)**0.2                                                   067
000234        C5=3.14159                                                      068
000235        C4=C5/4.0                                                       069
000237        X1=0.02                                                         070
000240        I4=INT(0.1/X1+0.5)
000244        W=0.0                                                           072
000244        U1=C9*U2                                                        073
000247        WRITE(6,8888)                                                   074
000252   8888 FORMAT(1H1)                                                     075
000252        WRITE(6,2000) (DATE(I),I=1,12)                                  076
000264   2000 FORMAT(1H ,50X,12A6/)                                           077
000264        WRITE(6,2010) (FUEL(I),I=1,12),(OXID(I),I=1,12)                 078
000304   2010 FORMAT(50H REGRESSION BEHAVIOR OF A CIRCULAR TUBE FUEL GRAIN//  079
               16H FUEL=,12A6/10H OXIDIZER=,12A6/)                            080
000304        WRITE(6,2020) D0,L,K2,K3,B,P0,M0,U0,U2,U1,C7,E2,K,K1,K4,K5,C8   081
000352        WRITE(6,2021) T1,X1,T3,T2,J                                     082
000370   2020 FORMAT(19H INITIAL CONDITIONS//15H DIAMETER     =,E14.5/        083
              1       15H LENGTH       =,E14.5/15H DENSITY      =,E14.5/      084
              2       15H EFF. H-SUB-V =,E14.5/15H BEE          =,E14.5/      085
              3       15H PRESSURE     =,E14.5/15H OXID. FLOW   =,E14.5/      086
              4       15H INLET TEMP.  =,E14.5/15H FLAME TEMP.  =,E14.5/      087
              5       15H RAD. TEMP.   =,E14.5/15H GAS CONST.   =,E14.5/      088
              6       15H WALL ABSORPT.=,E14.5/15H METAL PCT.   =,E14.5/      089
              7       15H PART. PCT.   =,E14.5/15H ZETA         =,E14.5/      090
              8       15H ZETA-1       =,E14.5/15H LAMBDA       =,E14.5)      091
000370   2021 FORMAT(15H DEL-T         =,E14.5/15H DEL-X/L      =,E14.5/
              1       15H PRINT TIME   =,E14.5/15H QUIT TIME    =,E14.5/
              2       15H CASE         =,I4)
000370        WRITE(6,8888)                                                   092
000374        WRITE(6,2000) (DATE(I),I=1,12)                                  093
000406        Q6=C1*C2*C3*(B)**0.23                                           094
```

```
000414          T4=0.0
000415          T5=0.0
000416          T=0.0
000420      155 X=X1
000421          I=1
000422          I1=I4
000424          M=M0
000426      165 IF(T.GT.0.0)GO TO 175
000431          D(I)=D0
000433      175 R3=(X*L)/(5.0*D(I))
000437          IF(R3.LE.1.0)GO TO 190
000442          IF(R3.GT.5.0)GO TO 200
000445          IF(R3.GT.1.0)GO TO 210
000447      190 E=D(I)*(1.0-0.21*(R3)**0.8)
000456          U=U0
000460          GO TO 220
000461      200 E=D(I)*(1.0-0.21)
000464          U=U2
000466          GO TO 220
000467      210 E=D(I)*(1.0-0.21)
000472          U=U0+((U2-U0)/4.0)*(R3-1.0)
000501      220 A=C4*(E)**2
000503          Q1=G6*(X)**(-0.2)*(M/A)**0.8
000515          Q3=C5*Q1*D0*X1*L
000522          R1=Q1/(K2*(1.0-K))
000526          GO TO (255,345,300),J
000535      255 IF(I.GT.1)GO TO 280
000541          M=M0+(1.0-K*K4/(1.0-K))*Q3
000550          M1=M0+Q3*1.0/(1.0-K)
000555          Q5=Q3
000556          N(I)=C6*C8*K/(1.0-K)*P0/U*1.0/M*Q3*(R3)**(-0.8)
000574          GO TO 366
000575      280 M=M+(1.0-K*K4/(1.0-K))*Q4
000604          M1=M1+Q4*1.0/(1.0-K)
000612          IF(R3.GT.1.0)GO TO 295
000615          N(I)=C6*C8*K/(1.0-K)*P0/U*1.0/M*Q5*(R3)**(-0.8)
000633          GO TO 366
000634      295 N(I)=C6*C8*K/(1.0-K)*P0/U*1.0/M*Q5
000646          GO TO 366
000646      300 IF(I.GT.1)GO TO 325
000652          M=M0+(1.0-K1-K1*K5)*Q3
000657          M1=M0+Q3
000660          Q5=Q3
000661          N(I)=C6*K1*P0/U*1.0/M*Q3*(R3)**(-0.8)
000674          GO TO 366
000675      325 M=M+(1.0-K1-K1*K5)*Q4
000702          M1=M1+Q4
000704          IF(R3.GT.1.0)GO TO 340
000707          N(I)=C6*K1*P0/U*1.0/M*Q5*(R3)**(-0.8)
000721          GO TO 366
000722      340 N(I)=C6*K1*P0/U*1.0/M*Q5
000731          GO TO 366
000731      345 IF(I.GT.1)GO TO 360
000735          M=M0+(1.0/(1.0-K))*Q3
000741          M1=M
000742          N(I)=C7*P0
000745          GO TO 366
000746      360 M=M+(1.0/(1.0-K))*Q4
```

```
000752          M1=M
000753          N(I)=C7*P0
000756      366 IF(J1.EQ.2)GO TO 371
000760          R2=R1
000761          UW=UWR/(1.0-UWR*ALOG(10.0*R2)/EF)
000771          TEE=TER*(M/MR*AR/A*(PR/P0)**NN*(UFR/U2)**(NN+2.0)*(1.0-CP*(UFR-UWR
               1     )/QF)/(1.0-CP*(U2-UW)/QF)*EXP(-UFR/U2))
001032          R2=R2*((2.0/TEE)**0.5*(1.0-1.0/TEE*(1.0-EXP(-TEE)))**0.5)
001051          GO TO 390
001052      371 IF(J.EQ.2)GO TO 384
001054          IF(N(I).GT.0.0)GO TO 375
001057          R2=R1
001057          UW=UWR/(1.0-UWR*ALOG(10.0*R2)/EF)
001067          TEE=TER*(M/MR*AR/A*(PR/P0)**NN*(UFR/U2)**(NN+2.0)*(1.0-CP*(UFR-UWR
               1     )/QF)/(1.0-CP*(U2-UW)/QF)*EXP(-UFR/U2))
001130          R2=R2*((2.0/TEE)**0.5*(1.0-1.0/TEE*(1.0-EXP(-TEE)))**0.5)
001147          GO TO 390
001150      375 IF(I.LT.I4)GO TO 382
001153          IF(I.GT.(8*I4))GO TO 382
001156          IF(I.EQ.I1)GO TO 382
001157          GO TO 387
001157      382 IF(T.EQ.T5)GO TO 590
001161          GO TO 387
001162      384 IF(I.GT.(2*I4))GO TO 387
001166          GO TO 375
001166      387 Q2=E1*E2/K3*E3*(U1)**4
001173          R2=Q1*(Q2/Q1+EXP(-Q2/Q1))/(K2*(1.0-K))
001206          UW=UWR/(1.0-UWR*ALOG(10.0*R2)/EF)
001215          TEE=TER*(M/MR*AR/A*(PR/P0)**NN*(UFR/U2)**(NN+2.0)*(1.0-CP*(UFR-UWR
               1     )/QF)/(1.0-CP*(U2-UW)/QF)*EXP(-UFR/U2))
001256          R2=R2*((2.0/TEE)**0.5*(1.0-1.0/TEE*(1.0-EXP(-TEE)))**0.5)
001275      390 Q4=C5*K2*(1.0-K)*R2*D(I)*X1*L
001305          Q5=Q5+Q4
001306          IF(I.EQ.I1)GO TO 495
001311          D(I)=D(I)+2.0*R2*T1
001314          IF(D(I).GT.D2)GO TO 795
001320      405 IF(X.GT.0.995)GO TO 425
001324          I=I+1
001325          X=X+X1
001327          GO TO 165
001327      425 IF(T.EQ.0.0)GO TO 450
001330          M3=(M1+M2)/2.0-M0
001334          W=W+M3*T1
001336          M2=M1
001337          IF(T.EQ.T4)GO TO 455
001342          T=T+T1
001342          IF(T.GT.T2)GO TO 800
001346          GO TO 155
001346      450 M2=M1
001347          IF(J1.EQ.2)GO TO 455
001352          J1=2
001353          GO TO 155
001353      455 WRITE(6,2030)
001357     2030 FORMAT(/13H    AVG. DEL-R,6X,8HWT. LOSS,6X,8HGAS FLOW,5X,
               1       10HTOTAL FLOW,7X,3HG-0)
001357          WRITE(6,2035)
001363     2035 FORMAT(10H         (IN),11X,4H(GM),8X,8H(LB/SEC),6X,8H(LB/SEC),
               1       3X,12H(LB/IN2-SEC))
```

```
001363          D6=(W/(C4*K2*L)+(D0)**2)**0.5
001373          AVGD=(D6-D0)/2.0
001376          WTL=W*453.6
001400          GSUB0=M0/(C4*(D6)**2)
001404          WRITE(6,2040) AVGD,WTL,M,M1,GSUB0
001421     2040 FORMAT(5E14.5//)
001421          T=T+T1
001423          T4=T4+T3
001425          IF(T.GT.T2)GO TO 800
001430          GO TO 155
001430      495 IF(T.EQ.T4)GO TO 506
001432          D(I)=D(I)+2.0*R2*T1
001437          I1=I1+I4
001441          GO TO 405
001441      506 IF(J1.EQ.2)GO TO 510
001443          GO TO 405
001444      510 IF(I1.EQ.I4)GO TO 520
001446          GO TO 535
001447      520 WRITE(6,2050) T
001455     2050 FORMAT(/11H       TIME/F10.0/)
001455          WRITE(6,2055)
001461     2055 FORMAT(25H                        TOTAL,7X,10HCONVECTIVE)
001461          WRITE(6,2060)
001465     2060 FORMAT(13H    DISTANCE,5X,8HREG RATE,6X,8HREG RATE,8X,
              1       5HDEL-R,7X,9HTUBE AREA,5X,9HFLOW AREA,5X,10HEMISSIVITY)
001465          WRITE(6,2065)
001471     2065 FORMAT(11H       (X/L),7X,8H(IN/SEC),6X,8H(IN/SEC),8X,4H(IN),
              1       9X,7H(IN**2),7X,7H(IN**2)/)
001471      535 DELR=(D(I)-D0)/2.0
001474          TUBEA=C4*(D(I))**2
001477          FLOWA=C4*(E)**2
001501          WRITE(6,2070) X,R2,R1,DELR,TUBEA,FLOWA,E3
001522     2070 FORMAT(7E14.5)
001522          D(I)=D(I)+2.0*R2*T1
001527          IF(D(I).GT.D2)GO TO 795
001533          I1=I1+I4
001534          GO TO 405
001535      590 T5=T5+(2.0*T3)
001540      600 R=D(I)/2.0
001542          R0=R-0.25
001544          Y1=3.14159/30.0
001545          Y2=ATAN(1.0/((R*R)/(R0*R0)-1.0)**0.5)
001556          E3=0.0
001557          J5=1
001561      633 K9=1.0
001562          Y=Y1/100.0
001565      635 Z=3.14159/2.0
001566          J4=1
001570      645 Y3=2.0*R*COS(Y)
001574          IF(Y.GT.Y2)GO TO 650
001600          S3=(Y3/2.0-(R0*R0-R*R*(SIN(Y))**2)**0.5)/SIN(Z)
001614      650 X3=J4*X1*L
001617          S4=Y3/SIN(Z)
001622          IF(Y.LT.Y2)GO TO 666
001625          K9=0.0
001626          S3=0.0
001627      666 IF(J5.EQ.1)GO TO 670
001631          S5=K9*EXP(-N(I-J4)*S3)-K9*EXP(-N(I-J4)*(S4-S3))+EXP(-N(I-J4)*S4)
```

```
001656            GO TO 675
001657        670 S5=K9*EXP(-N(I+J4)*S3)-K9*EXP(-N(I+J4)*(S4-S3))+EXP(-N(I+J4)*S4)
001704        675 S6=(1.0-S5)*(SIN(Z))**2*COS(Y)
001714            Z1=(Y3*X1*L)/((X3)**2+(Y3)**2)
001721            S7=S6*Z1*Y1*2.0/3.14159
001724            E3=E3+S7/1.06988
001727            Z=Z-Z1
001731            J4=J4+1
001733            IF(J5.EQ.1)GO TO 705
001735            IF(J4.GT.I)GO TO 720
001740            IF(J4.GT.10)GO TO 720
001742            GO TO 645
001742        705 IF(J4.GT.(1.0/X1-I))GO TO 720
001751            IF(J4.GT.10)GO TO 720
001754            GO TO 645
001754        720 Y=Y+Y1
001756            IF(Y.GT.(3.14159/2.0))GO TO 745
001761            GO TO 635
001761        745 IF(J5.EQ.2)GO TO 750
001763            J5=2
001764            GO TO 633
001765        750 GO TO 387
001766        795 WRITE(6,2080)
001772       2080 FORMAT(/37H SPECIFIED EXTERNAL DIAMETER EXCEEDED/)
001772        800 GO TO 10
001773        850 STOP
001775            END
```

MAR 4 1970

REGRESSION BEHAVIOR OF A CIRCULAR TUBE FUEL GRAIN

FUEL=PU
OXIDIZER=OXYGEN

INITIAL CONDITIONS

DIAMETER	=	1.05000E+00
LENGTH	=	1.20000E+01
DENSITY	=	4.27014E-02
EFF. H-SUB-V	=	6.30000E+02
BEE	=	9.10000E+00
PRESSURE	=	5.00000E+01
OXID. FLOW	=	4.33000E-02
INLET TEMP.	=	5.40000E+02
FLAME TEMP.	=	6.11863E+03
RAD. TEMP.	=	3.59164E+03
GAS CONST.	=	3.00000E-03
WALL ABSORPT.	=	9.00000E-01
METAL PCT.	=	2.00000E-01
PART. PCT.	=	0.
ZETA	=	8.88000E-01
ZETA-1	=	0.
LAMBDA	=	1.88800E+00
DEL-T	=	2.50000E-01
DEL-X/L	=	2.00000E-02
PRINT TIME	=	1.00000E+00
QUIT TIME	=	5.00000E+00
CASE	=	1

TIME
0

DISTANCE (X/L)	TOTAL REG RATE (IN/SEC)	CONVECTIVE REG RATE (IN/SEC)	DEL-R (IN)	TUBE AREA (IN**2)	FLOW AREA (IN**2)	EMISSIVITY
1.00000E-01	7.91429E-03	1.36723E-02	0.	8.65901E-01	7.57831E-01	4.98394E-01
2.00000E-01	7.31592E-03	1.31353E-02	0.	8.65901E-01	6.82387E-01	4.98394E-01
3.00000E-01	6.99811E-03	1.32913E-02	0.	8.65901E-01	6.17856E-01	4.98394E-01
4.00000E-01	6.78799E-03	1.37389E-02	0.	8.65901E-01	5.60467E-01	4.98394E-01
5.00000E-01	6.61644E-03	1.36930E-02	0.	8.65901E-01	5.40409E-01	4.98394E-01
6.00000E-01	6.47172E-03	1.33573E-02	0.	8.65901E-01	5.40409E-01	4.98394E-01
7.00000E-01	6.35357E-03	1.30982E-02	0.	8.65901E-01	5.40409E-01	4.98394E-01
8.00000E-01	6.25408E-03	1.28926E-02	0.	8.65901E-01	5.40409E-01	4.98394E-01
9.00000E-01	6.16832E-03	1.27264E-02	0.	8.65901E-01	5.40409E-01	4.98394E-01
1.00000E+00	6.09307E-03	1.25901E-02	0.	8.65901E-01	5.40409E-01	4.98394E-01

AVG. DEL-R (IN)	WT. LOSS (GM)	GAS FLOW (LB/SEC)	TOTAL FLOW (LB/SEC)	G-0 (LB/IN2-SEC)
0.	0.	5.07208E-02	5.52229E-02	5.00057E-02

TIME
1

DISTANCE (X/L)	TOTAL REG RATE (IN/SEC)	CONVECTIVE REG RATE (IN/SEC)	DEL-R (IN)	TUBE AREA (IN**2)	FLOW AREA (IN**2)	EMISSIVITY
1.00000E-01	7.89751E-03	1.33308E-02	7.90782E-03	8.92182E-01	7.82113E-01	4.98394E-01
2.00000E-01	7.30639E-03	1.28209E-02	7.31220E-03	8.90189E-01	7.03482E-01	4.98394E-01
3.00000E-01	6.98960E-03	1.29764E-02	6.99478E-03	8.89128E-01	6.36888E-01	4.98394E-01
4.00000E-01	6.77832E-03	1.34122E-02	6.78423E-03	8.88424E-01	5.77905E-01	4.98394E-01
5.00000E-01	6.60929E-03	1.34291E-02	6.61367E-03	8.87854E-01	5.54110E-01	4.98394E-01
6.00000E-01	6.46648E-03	1.31072E-02	6.46967E-03	8.87374E-01	5.53810E-01	4.98394E-01
7.00000E-01	6.34976E-03	1.28590E-02	6.35207E-03	8.86981E-01	5.53565E-01	4.98394E-01
8.00000E-01	6.25137E-03	1.26624E-02	6.25299E-03	8.86650E-01	5.53358E-01	4.98394E-01
9.00000E-01	6.16648E-03	1.25037E-02	6.16757E-03	8.86365E-01	5.53180E-01	4.98394E-01
1.00000E+00	6.09193E-03	1.23738E-02	6.09258E-03	8.86115E-01	5.53024E-01	4.98394E-01

AVG. DEL-R (IN)	WT. LOSS (GM)	GAS FLOW (LB/SEC)	TOTAL FLOW (LB/SEC)	G-0 (LB/IN2-SEC)
7.04133E-03	5.43491E+00	5.07943E-02	5.53410E-02	4.86909E-02

TIME
2

DISTANCE (X/L)	TOTAL REG RATE (IN/SEC)	CONVECTIVE REG RATE (IN/SEC)	DEL-R (IN)	TUBE AREA (IN**2)	FLOW AREA (IN**2)	EMISSIVITY
1.00000E-01	7.88208E-03	1.30037E-02	1.57997E-02	9.18803E-01	8.06732E-01	4.98272E-01
2.00000E-01	7.29792E-03	1.25190E-02	1.46156E-02	9.14784E-01	7.24877E-01	4.98272E-01
3.00000E-01	6.98210E-03	1.26739E-02	1.39817E-02	9.12636E-01	6.56194E-01	4.98272E-01
4.00000E-01	6.76970E-03	1.30985E-02	1.35594E-02	9.11206E-01	5.95594E-01	4.98272E-01
5.00000E-01	6.60260E-03	1.31740E-02	1.32206E-02	9.10060E-01	5.67969E-01	4.98272E-01
6.00000E-01	6.46161E-03	1.28652E-02	1.29345E-02	9.09093E-01	5.67365E-01	4.98272E-01
7.00000E-01	6.34626E-03	1.26274E-02	1.27007E-02	9.08303E-01	5.66872E-01	4.98272E-01
8.00000E-01	6.24891E-03	1.24393E-02	1.25036E-02	9.07637E-01	5.66456E-01	4.98272E-01
9.00000E-01	6.16484E-03	1.22878E-02	1.23336E-02	9.07063E-01	5.66098E-01	4.98272E-01
1.00000E+00	6.09093E-03	1.21641E-02	1.21843E-02	9.06559E-01	5.65784E-01	4.98272E-01

AVG. DEL-R (IN)	WT. LOSS (GM)	GAS FLOW (LB/SEC)	TOTAL FLOW (LB/SEC)	G-0 (LB/IN2-SEC)
1.40594E-02	1.09239E+01	5.08687E-02	5.54605E-02	4.74313E-02

TIME
3

DISTANCE (X/L)	TOTAL REG RATE (IN/SEC)	CONVECTIVE REG RATE (IN/SEC)	DEL-R (IN)	TUBE AREA (IN**2)	FLOW AREA (IN**2)	EMISSIVITY
1.00000E-01	7.86943E-03	1.26901E-02	2.36769E-02	9.45764E-01	8.31689E-01	4.98272E-01
2.00000E-01	7.29191E-03	1.22289E-02	2.19111E-02	9.39686E-01	7.46575E-01	4.98272E-01
3.00000E-01	6.97695E-03	1.23833E-02	2.09617E-02	9.36427E-01	6.75776E-01	4.98272E-01
4.00000E-01	6.76338E-03	1.27972E-02	2.03266E-02	9.34250E-01	6.13535E-01	4.98272E-01
5.00000E-01	6.59762E-03	1.29274E-02	1.98213E-02	9.32519E-01	5.81985E-01	4.98272E-01
6.00000E-01	6.45837E-03	1.26311E-02	1.93948E-02	9.31060E-01	5.81074E-01	4.98272E-01
7.00000E-01	6.34430E-03	1.24032E-02	1.90461E-02	9.29867E-01	5.80330E-01	4.98272E-01
8.00000E-01	6.24794E-03	1.22232E-02	1.87521E-02	9.28862E-01	5.79703E-01	4.98272E-01
9.00000E-01	6.16464E-03	1.20786E-02	1.84983E-02	9.27996E-01	5.79162E-01	4.98272E-01
1.00000E+00	6.09134E-03	1.19608E-02	1.82753E-02	9.27234E-01	5.78687E-01	4.98272E-01

AVG. DEL-R (IN)	WT. LOSS (GM)	GAS FLOW (LB/SEC)	TOTAL FLOW (LB/SEC)	G-0 (LB/IN2-SEC)
2.10561E-02	1.64678E+01	5.09454E-02	5.55838E-02	4.62236E-02

TIME
4

DISTANCE (X/L)	TOTAL REG RATE (IN/SEC)	CONVECTIVE REG RATE (IN/SEC)	DEL-R (IN)	TUBE AREA (IN**2)	FLOW AREA (IN**2)	EMISSIVITY
1.00000E-01	7.84975E-03	1.23890E-02	3.15421E-02	9.73073E-01	8.56991E-01	4.96936E-01
2.00000E-01	7.27890E-03	1.19497E-02	2.92012E-02	9.64905E-01	7.68581E-01	4.96936E-01
3.00000E-01	6.96521E-03	1.21032E-02	2.79372E-02	9.60508E-01	6.95638E-01	4.96936E-01
4.00000E-01	6.75102E-03	1.25068E-02	2.70881E-02	9.57561E-01	6.31733E-01	4.96936E-01
5.00000E-01	6.58635E-03	1.26879E-02	2.64173E-02	9.55235E-01	5.96162E-01	4.96936E-01
6.00000E-01	6.44872E-03	1.24033E-02	2.58522E-02	9.53278E-01	5.94941E-01	4.96936E-01
7.00000E-01	6.33586E-03	1.21847E-02	2.53900E-02	9.51679E-01	5.93943E-01	4.96936E-01
8.00000E-01	6.24042E-03	1.20125E-02	2.49999E-02	9.50331E-01	5.93101E-01	4.96936E-01
9.00000E-01	6.15785E-03	1.18742E-02	2.46631E-02	9.49167E-01	5.92375E-01	4.96936E-01
1.00000E+00	6.08514E-03	1.17620E-02	2.43671E-02	9.48145E-01	5.91737E-01	4.96936E-01

AVG. DEL-R (IN)	WT. LOSS (GM)	GAS FLOW (LB/SEC)	TOTAL FLOW (LB/SEC)	G-0 (LB/IN2-SEC)
2.80333E-02	2.20674E+01	5.10153E-02	5.56961E-02	4.50646E-02

TIME
5

DISTANCE (X/L)	TOTAL REG RATE (IN/SEC)	CONVECTIVE REG RATE (IN/SEC)	DEL-R (IN)	TUBE AREA (IN**2)	FLOW AREA (IN**2)	EMISSIVITY
1.00000E-01	7.84062E-03	1.21002E-02	3.93883E-02	1.00070E+00	8.82613E-01	4.96936E-01
2.00000E-01	7.27590E-03	1.16815E-02	3.64789E-02	9.90413E-01	7.90874E-01	4.96936E-01
3.00000E-01	6.96294E-03	1.18343E-02	3.49015E-02	9.84856E-01	7.15762E-01	4.96936E-01
4.00000E-01	6.74759E-03	1.22284E-02	3.38377E-02	9.81117E-01	6.50173E-01	4.96936E-01
5.00000E-01	6.58324E-03	1.24572E-02	3.30024E-02	9.78187E-01	6.10486E-01	4.96936E-01
6.00000E-01	6.44719E-03	1.21839E-02	3.23003E-02	9.75726E-01	6.08951E-01	4.96936E-01
7.00000E-01	6.33549E-03	1.19743E-02	3.17256E-02	9.73715E-01	6.07696E-01	4.96936E-01
8.00000E-01	6.24094E-03	1.18095E-02	3.12405E-02	9.72019E-01	6.06637E-01	4.96936E-01
9.00000E-01	6.15905E-03	1.16775E-02	3.08213E-02	9.70555E-01	6.05723E-01	4.96936E-01
1.00000E+00	6.08687E-03	1.15706E-02	3.04528E-02	9.69268E-01	6.04920E-01	4.96936E-01

AVG. DEL-R (IN)	WT. LOSS (GM)	GAS FLOW (LB/SEC)	TOTAL FLOW (LB/SEC)	G-0 (LB/IN2-SEC)
3.49873E-02	2.77192E+01	5.10949E-02	5.58239E-02	4.39523E-02

REFERENCES

1. Marxman, G. A., Wooldridge, C. E., and Muzzy, R. J., "Fundamentals of Hybrid Boundary Layer Combustion," Heterogeneous Combustion, Progress in Astronautics and Aeronautics, Vol. 15, Academic Press, New York, 1964, p. 485.

2. Marxman, G. A., and Gilbert, M., "Turbulent Boundary Layer Combustion in the Hybrid Rocket," Ninth Symposium (International) on Combustion, Academic Press, New York, 1963, p. 371.

3. Barrere, M., and Moutet, A., "La Propulsion par Fusees Hybrides," presented at the International Astronautical Congress, Paris, September 1963.

4. Green, L., Jr., "Introductory Considerations of Hybrid Rocket Combustion," Heterogeneous Combustion, Progress in Astronautics and Aeronautics, Vol. 15, Academic Press, New York, 1964, p. 451.

5. Marxman, G. A., and Wooldridge, C. E., "Research on the Combustion Mechanism of Hybrid Rockets," presented at the Combustion and Propulsion Panel, AGARD, NATO, San Diego, California, April 22-24, 1965.

6. Marxman, G. A., "Combustion in the Turbulent Boundary Layer on a Vaporizing Surface," Tenth Symposium (International) on Combustion, The Combustion Institute, Pittsburgh, 1965, p. 1337.

7. Wooldridge, C. E., Marxman, G. A., and Kier, R. J., "Investigation of Combustion Instability in Hybrid Rockets", Final Report, NASA Contract NAS 1-7310, Stanford Research Institute, September 1969.

8. Smoot, L. D., and Price, C. F., "Regression Rate Mechanism of Nonmetalized Hybrid Fuel Systems," AIAA J. 3, 1408-1413 (1965).

9. ___________, "Regression Rates of Metalized Hybrid Fuel Systems," AIAA J. 4, 910-915 (1966).

10. ___________, "Pressure Dependence of Hybrid Fuel Regression Rates," AIAA J. 5, 102-106 (1967).